^{14}N Coupling Parameters in Oxovanadium(IV)−Amine, −Imine, and −Isothiocyanate Complexes Studied by Electron Spin Echo Envelope Modulation Spectroscopy

Kouichi Fukui,* Hiroaki Ohya-Nishiguchi, and Hitoshi Kamada

Institute for Life Support Technology, Yamagata Technopolis Foundation, Matsuei 2-2-1, Yamagata 990, Japan

Received December 6, 1996[⊗]

Electron spin echo envelope modulation (ESEEM) spectroscopy has been applied to several nitrogen-coordinated oxovanadium(IV) complexes. Results for two amine-nitrogen complexes, VO(edda) and VO(gly)$_2$, two imine-nitrogen complexes, VO(salen) and VO(salophen), and one isothiocyanate complex, VO(NCS)$_4^{2-}$, are presented. [H$_2$edda = ethylenediamine-*N*,*N*′-diacetic acid, gly$^-$ = glycinate, H$_2$salen = *N*,*N*′-bis(salicylidene)ethylenediamine, and H$_2$salophen = *N*,*N*′-bis(salicylidene)-*o*-phenylenediamine.] The ^{14}N hyperfine coupling (HFC) and quadrupole coupling (NQC) parameters have been determined from computer simulation of the two-pulse and three-pulse ESEEM data recorded at some selected field positions. Resulting NQC parameters are e^2qQ = 3.1 MHz (VO(edda)), 2.7 MHz (VO(gly)$_2$), 2.4 MHz (VO(salen)), 2.6 MHz (VO(salophen), and 1.0 MHz (VO(NCS)$_4^{2-}$). The isotropic HFC parameters, $|A_{iso}|$, show a good correlation to the nitrogen type as 4.98 MHz (VO(edda)), 5.10 MHz (VO(gly)$_2$), 5.83 MHz (VO(salen)), 5.78 MHz (VO(salophen)), and 7.47 MHz (VO(NCS)$_4^{2-}$). The isotropic and anisotropic parts of the HFC parameters are analyzed in terms of the indirect spin transfer mechanism. The analysis has given good quantitative agreements, supporting the validity of this mechanism. According to the mechanism, the isotropic part of HFC depends essentially on two factors, the degree of the (negative) polarization of the nitrogen lone-pair sp^n-hybrid orbital and the s orbital content of this orbital. The analysis has shown that the polarization is invariably around −1%. Thus, the good correlation can be attributed to the distinct difference of the s-orbital contents between nitrogen types.

Introduction

Vanadium is known as a biologically essential trace element,[1] and is found, for example, in some haloperoxidases,[2−4] a nitrogenase,[5] blood cells of tunicates,[6] *etc*. Furthermore, increasing attention is paid to vanadium because of its insulin-mimic activity.[7−11] Oxovanadium(IV) ion has a paramagnetic d^1 electron configuration. Thus, various information can be gained by EPR[12] spectroscopy, which makes oxovanadium(IV) ion a useful EPR spectroscopic probe.[13] For example, usefulness of the $A_{||}(^{51}V)-g_{||}$ plot has been demonstrated in identifying the donor atom combination around the VO^{2+} ion.[13] On the other hand, ESEEM spectroscopy, which is based on the pulsed EPR technique, has been developing. This spectroscopy provides a unique means to probe very weak couplings between the unpaired electron and nearby nuclei. The magnitudes of the V−N couplings are in a range suitable for ESEEM investigation. Therefore further insights into the VO^{2+}-site structures (such as V−N distances and the orientations and electronic structures of nitrogen-containing ligands) are expected to be obtained from ESEEM studies of VO^{2+} complexes and VO-containing proteins.

ESEEM results reported so far for ^{14}N nuclei coordinated equatorially to VO^{2+} ion have demonstrated a distinctive difference between amine and imine nitrogens in the magnitudes of HFC: The HFC parameters reported for V−N$_{amine}$ couplings generally appear around 5 MHz as $|A_{||}|$ = 4.4−5.4 MHz and $|A_{\perp}|$ = 3.6−4.9 MHz for amine nitrogen adducts of VO(acac)$_2$,[14] $|A_{iso}|$ = 5.0 MHz for VO(gly)$_2$,[15] and 4.7 MHz for VO−NH$_3$ on a silica-supported vanadium oxide.[16] VO−*S*-adenosylmethionine synthase complexes were reported to exhibit ^{14}N ESEEM signals of $|A_{iso}|$ = 4.3−5.5 MHz, which were assigned to lysine ϵ-amine and *S*-adenosylmethionin α-amine with the help of selective ^{15}N labeling.[17] On the other hand, the HFC parameters reported for V−N$_{imine}$ couplings are generally found in the range ∼6−∼7 MHz as $|A_{||}|$ = 6 MHz and $|A_{\perp}|$ = 5.6

[⊗] Abstract published in *Advance ACS Abstracts*, October 15, 1997.

(1) Schwartz, K.; Milne, D. B. *Science* **1971**, *174*, 426−428.
(2) De Boer, E.; Boon, K.; Wever, R. *Biochemistry* **1988**, *27*, 1629−1635.
(3) De Boer, E.; Keijzers, C. P.; Klaassen, A. A. K.; Reijerse, E. J.; Collison, D.; Garner, C. D.; Wever, R. *FEBS Lett.* **1988**, *235*, 93−97.
(4) Van Schijndel, J. W. P. M.; Vollenbroek, E. G. M.; Wever, R. *Biochim. Biophys. Acta* **1993**, *1161*, 249−256.
(5) (a) Hales, B. J.; Case, E. E.; Morningstar, J. J.; Dzeda, M. F.; Mauterer, L. A. *J. Biochemistry* **1986**, *25*, 7251−7255. (b) Robson, R. L.; Eady, R. R.; Richardson, T. H.; Miller, R. W.; Hawkins, M.; Postgate, J. R. *Nature* **1986**, *322*, 388−390.
(6) Frank, P.; Hedman, B.; Carlson, R. M. K.; Hodgson, K. O. *Inorg. Chem.* **1994**, *33*, 3794−3803 and references cited therein.
(7) Dubyak, G. R.; Kleinzeller, A. *J. Biol. Chem.* **1980**, *255*, 5306−5312.
(8) Shechter, Y.; Karlish, S. J. D. *Nature* **1980**, *284*, 556−558.
(9) Sun, Y.; James, B. R.; Rettig, S. J.; Orvig, C. *Inorg. Chem*. **1996**, *35*, 1667−1673.
(10) Sakurai, H.; Tsuchiya, M.; Nukatsuka, M.; Sofue, M.; Kawada, J. *J. Endocrinol.* **1990**, *126*, 451−459.
(11) Fukui, K.; Ohya-Nishiguchi, H.; Nakai, M.; Sakurai, H.; Kamada, H. *FEBS Lett.* **1995**, *368*, 31−35.
(12) Abbreviations: CW, continuous wave; ENDOR, electron nuclear double resonance; EPR, electron paramagnetic resonance; ESEEM, electron spin echo envelope modulation; HFC, hyperfine coupling; LPSVD, linear prediction singular value decomposition; NQC, nuclear quadrupole coupling; NZC, nuclear Zeeman coupling; acac$^-$, acetylacetonate; H$_2$edda, ethylenediaminediacetic acid; gly$^-$, glycinate; meox$^-$, 2-methyl-8-quinolinolate; H$_2$oep, octaethylporphyrin; H$_2$salen, *N*,*N*′-bis(salicylidene)ethylenediamine; H$_2$salophen, *N*,*N*′-bis(salicylidene)-*o*-phenylenediamine; mim, 1-methylimidazole.
(13) Chasteen, N. D. In *Biological Magnetic Resonance*; Berliner, L. J., Reuben, J., Eds.; Plenum: New York, 1981; Vol. 3, pp 53−119.
(14) Astashkin, A. V.; Dikanov, S. A.; Tsvetkov, Yu. D. *J. Struct. Chem.* **1985**, *26*, 363−368.
(15) Tipton, P. A.; McCracken, J., Cornelious, J. B.; Peisach, J. *Biochemistry* **1989**, *28*, 5720−5728.
(16) Larsen, S. C.; Singel, D. J. *J. Phys. Chem.* **1992**, *96*, 9007−9013.
(17) Zhang, C.; Markham, G. D.; LoBrutto, R. *Biochemistry* **1993**, *32*, 9866−9873.

S0020-1669(96)01462-0 CCC: $14.00

MHz for imine nitrogen adducts of $VO(acac)_2$;[14] $|A_{iso}| = 6.03$ MHz for $VO(meox)_2$;[18,19] 6.43 MHz for $VO(min)_4Cl^+$;[18,19] $|A| = 7.1$ and 7.6 MHz for pyridine and imidazole adducts of VO-(hexafluoroacetylacetonate)$_2$, respectively;[20] and $|A_{iso}| = 7.2$ and 7.3 MHz for VO−porphyrin complexes.[21] Two-dimensional ESEEM study of a VO-histidine complex was recently reported,[22] demonstrating the distinctive difference between the α-amine nitrogen ($|A| = 5.0$ MHz) and the imidazole imine nitrogen ($|A| = 6.3$ MHz). Consequently, it seems reasonable to expect that ESEEM spectroscopy can be used to identify the types of nitrogens coordinated to VO^{2+} ion. In fact, numerous studies have been undertaken along this line: For example, previous ESEEM results of VO−pyruvate kinase complexes indicate equatorial coordination of amine nitrogen to the VO^{2+} ion.[15] Equatorial coordination of imine nitrogen was demonstrated to occur in reduced vanadium bromoperoxidase,[3] VO−lactoferrin and −transferrin complexes, [20] VO−ferritin,[23] VO−D-xylose isomerase,[24] *etc*. Concurrent coordination of amine and imine nitrogens was deduced from the 1D- and 2D-ESEEM results of a VO−ATPase complex.[25]

Although the correlation between ^{14}N HFC parameters and nitrogen types seems experimentally established, its origin is not fully understood. Because of its practical importance, it is desirable to clarify the origin of the correlation. This will further provide insights into possible exceptions to the correlation rule. It has been supposed that the correlation would be related with the difference in sp^n hybridization between amine and imine nitrogens. However no attempts have been made to check the validity of this idea. For this purpose, examination of the other sp^n-hybrid system (i.e. sp-hybrid system) would be effective. If the idea that the hybridization is a key factor of HFC is valid, the HFC parameter of sp-hybrid nitrogens must be also distinctively different from those of the sp^3-hybrid amine nitrogens and sp^2-hybrid imine nitrogens, which turns out to be true as we show in this paper.

In the present paper, we report ESEEM results of several nitrogen-coordinated VO^{2+} complexes, two amine-nitrogen complexes, VO(edda) and $VO(gly)_2$, two imine-nitrogen complexes, VO(salen) and VO(salophen), and one sp-hybrid isothiocyanate complex, $VO(NCS)_4^{2-}$. We have found that the isotropic HFC parameter of the isothiocyanate nitrogen is distinctively larger (in magnitude) than those of the amine and imine nitrogens, which not only extends the correlation rule to a new nitrogen type but also allows detailed discussion on the origin of the good correlation.

Experimental Section

Materials. Reagents were purchased from Wako (salicylaldehyde), Sigma (H_2edda), and Kanto Chemicals (other reagents) and used without further purification. VO(edda) was prepared by mixing aqueous solutions of $VOSO_4{\cdot}xH_2O$ ($x = 3$ is assumed), H_2edda, and NaOH. Violet crystals formed after storage of the mixture in a refrigerator for a few days. For EPR measurements, crystals were dissolved in distilled water, and an equal volume of ethylene glycol was added for good glass formation (the final concentration of VO(edda) was 5 mM). Aqueous solutions of $VO(gly)_2$ were prepared on the basis of previous kinetic studies of VO−glycine systems.[26,27] Accordingly, aqueous solutions containing $VOSO_4{\cdot}xH_2O$ and glycine were mixed, and the pH of the mixture was adjusted to 7 with NaOH. The formation of $VO(gly)_2$ was checked by visible absorption.[28] To a sample of the aqueous solution, an equal volume of ethylene glycol was added for EPR measurements (final concentration of vanadium was about 5 mM). VO(salen) and VO(salophen) were prepared according to an analogous method described for VO(dithio-salen).[29] The complexes VO(salen) and VO(salophen) were recrystalized from CH_2Cl_2/ethanol mixed solvent and acetonitrile, respectively. The crystals were dissolved in DMF/toluene (1:1 v/v) mixed solvent for EPR measurements. (The concentrations were 5 mM). MeOH solutions of $VO(NCS)_4^{2-}$ were prepared according to a slightly modified method reported previously.[30] We employed NaSCN as a source of SCN^- and MeOH as solvent. The concentration of vanadium in EPR samples was about 5 mM in MeOH/ethylene glycol (3:1) mixed solvent.

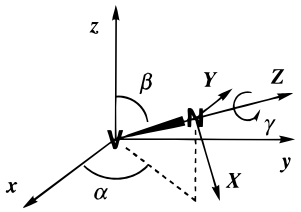

Figure 1. Definition of the Euler angles, α, *β*, and *γ*, connecting between the molecular axes *xyz* (**g**-tensor axes) and the nitrogen local axes *XYZ* (HFC **A** and NQC **Q** tensor axes). The local axes for the HFC and NQC axes may not be coincident, so that thus occurring two sets of Euler angles are distinguished as (α_A, β_A, γ_A) and (α_Q, β_Q, γ_Q) in the text.

EPR Measurements. CW EPR and ESEEM measurements were carried out on a JEOL RE-3X spectrometer equipped with a JEOL ES-PX1000 pulse EPR unit. The two-pulse sequence ($\pi/2-\tau-\pi-\tau-$echo) and the three-pulse sequence ($\pi/2-\tau-\pi/2-T-\pi/2-\tau-$echo) were applied with pulse widths of $t_{\pi/2} = 15$ ns and $t_\pi = 30$ ns. Measurements were generally made at liquid N_2 temperature (77 K). For the complexes studied here, the echo intensity was sufficiently strong and the relaxation time was sufficiently long at 77 K. In fact, although we measured VO(oep) at 10 K, the quality of the data was not very different from that obtained at 77 K. ESEEM time-domain data typically with a 20 ns interval were collected on a JEOL ESPRIT330 computer. Prior to cosine FFT, linear prediction singular value decomposition (LPSVD) was applied to reconstruct the data lost to instrumental dead time.[31]

Computer simulation was performed on the basis of the spin density formalism of Mims.[32,33] The system treated here can be described with the spin Hamiltonian for $S = {}^1/_2$ and $I_i = 1$ ($i = 1, 2, ..., N$)

$$H = \mu_B \mathbf{S}\cdot\mathbf{g}\cdot\mathbf{B} + \sum_i (h\mathbf{S}\cdot\mathbf{A}_i\cdot\mathbf{I}_i + h\mathbf{I}_i\cdot\mathbf{Q}_i\cdot\mathbf{I}_i - \mu_N g_N \mathbf{I}_i\cdot\mathbf{B}) \quad (1)$$

where the symbols have usual meanings. The ^{14}N HFC tensor **A** and ^{14}N NQC tensor **Q** have sets of principal values (A_X, A_Y, A_Z) and (Q_X, Q_Y, Q_Z), respectively. The principal axes *XYZ* of the **A** and **Q** tensors are connected with the molecular axes (**g**-tensor axes) *xyz* by the sets of Euler angles (α_A, β_A, γ_A) and (α_Q, β_Q, γ_Q), respectively (Figure 1).

(18) Reijerse, E. J.; Shane, J.; de Bohr, E.; Collison, D. In *Electron Magnetic Resonance of Disordered Systems*; Yordanov, N. D., Ed.; World Scientific: Singapore, 1989; pp 189−204.
(19) Reijerse, E. J.; Shane, J.; de Bohr, E.; Höffer, P.; Collison, D. In *Electron Magnetic Resonance of Disordered Systems*; Yordanov, N. D., Ed.; World Scientific: Singapore, 1991; pp 253−271.
(20) Eaton, S. S.; Dubach, J.; More, K. M.; Eaton, G. R.; Thurman, G.; Ambruso, D. R. *J. Biol. Chem.* **1989**, *264*, 4776−4781.
(21) Fukui, K.; Ohya-Nishiguchi, H.; Kamada, H. *J. Phys. Chem.* **1993**, *97*, 11858−11860.
(22) Dikanov, S. A.; Samoilova, R. I.; Smieja, J. A.; Bowman, M. K. *J. Am Chem. Soc.* **1995**, *117*, 10579−10580.
(23) Gerfen, G. J.; Hanna, P. M.; Chasteen, N. D.; Singel, D. J. *J. Am. Chem. Soc.* **1991**, *113*, 9513−9519.
(24) Dikanov, S. A.; Tyryshkin, A. M.; Hüttermann, J.; Bogumil, R.; Witzel, H. *J. Am. Chem. Soc.* **1995**, *117*, 4976−4986.
(25) Buy, C.; Matsui, T.; Andrianambinintsoa, S.; Sigalat, C.; Girault, G.; Zimmermann, J.-L. *Biochemistry* **1996**, *35*, 14281−14293.
(26) Tomiyasu, H.; Dreyer, K.; Gordon, G. *Inorg. Chem.* **1972**, *11*, 2409−2414.
(27) Tomiyasu, H.; Gordon, G. *Inorg. Chem.* **1976**, *15*, 870−874.
(28) Tomiyasu, H.; Gordon, G. *J. Coord. Chem.* **1973**, *3*, 47−56.
(29) Dutton, J. C.; Fallen, G. D.; Murray, K. S. *Inorg. Chem.* **1988**, *27*, 34−38.
(30) Hazell, A. C. *J. Chem. Soc.* **1963**, *30*, 5745−5752.
(31) (a) Barkhuijsen, H.; De Beer, R.; Bovée, W. M. M. J.; Van Ormondt, D. *J. Magn. Reson.* **1985**, *61*, 465−481. (b) Stephenson, D. S. *Prog. NMR Spectrosc.* **1988**, *20*, 515−626.
(32) Mims, W. B. *Phys. Rev. B* **1972**, *5*, 2409−2419.
(33) Mims, W. B. *Phys. Rev. B* **1972**, *6*, 3543−3545.

We may also use A_x, A_y, and A_z (and Q_x, Q_y, and Q_z), where A_z, for example, denotes the principal component corresponding to the **A** tensor axis parallel or most parallel to the g_z axis.

Theoretical Background. For ^{14}N nuclei coordinated equatorially to VO^{2+} ion, the size of HFC is of the order of 5−8 MHz, which is larger than those of NQC (1−2 MHz) and NZC (∼1 MHz at X band). Then the nuclear spin states in the two $m_S = \pm^1/_2$ manifolds can be regarded approximately as the Zeeman states $|m_I\rangle = |-1\rangle$, $|0\rangle$, and $|1\rangle$ quantized along the local field due to HFC. Thus each manifold exhibits one double-quantum transition $\nu_{dq\pm}$ ($\Delta m_I = 2$) and two single-quantum transitions $\nu_{sq\pm}^{(1)}$ and $\nu_{sq\pm}^{(2)}$ ($\Delta m_I = 1$). This is in contrast to the situation under "exact cancellation",[34] where one of the manifolds splits into the "pure quadrupole" states and exhibits the quadrupole transitions, ν_0, ν_+, and ν_-. Under the condition of strong HFC, the double-quantum transitions usually participate as the most strong modulations in ESEEM patterns.[34] The modulations due to the single-quantum transitions are usually weak and broad and even not observed[34] in contrast to the situation in ENDOR spectroscopy.[35] Besides the modulations due to these fundamental transitions, two-pulse ESEEM contains the "sum and difference" frequency modulations, where the sum and difference are about one fundamental frequency from one manifold and the other from the other manifold such as $\nu_{dq+} \pm \nu_{dq-}$, $\nu_{dq+} \pm \nu_{sq-}^{(1)}$, $\nu_{dq+} \pm \nu_{sq-}^{(2)}$, *etc*.[32,33] The "sum and difference" modulations are often in counter-phase and appear as negative-amplitude lines in the cosine FT spectra.[34,36] Finally, in the case of multiple nitrogen coordination, another type of "sum and difference" combinations can arise in both two-pulse and three-pulse ESEEM from the interactions between different nuclear spins connected by one electron spin.[32]

The expected frequencies and amplitudes of the above listed modulation components can be calculated using the Mims formula.[32,33] Numerous studies have been made to characterize the quantitative aspects of ESEEM of the $I = 1$ system under various conditions.[34,36−40] In the following, we summarize some of the important results relevant in the interpretation of the ESEEM results presented here. To keep equations simple, we will confine ourselves to a simple case where coincidence occurs about all the relevant orientations, the orientations of applied field and principal axes of the **g**, ^{14}N HFC **A**, and ^{14}N NQC **Q** tensors. The equations thus simplified still retain many important features reported previously[34,36−40] as shown below and would suffice the initial analyses of the observed spectra. Furthermore, in many VO^{2+} complexes, the g_z axis is most likely parallel to the V═O direction, $g_x \approx g_y$, and the coordinating nitrogens are often situated in the equatorial plane. Thus the coincidence of all the relevant orientations will actually occur when the g_z ($=g_{\parallel}$) line of the CW EPR spectrum is selectively excited for such VO^{2+} complexes.

When the orientations of applied field and principal axes (e.g., ζ axes) of the **g**, **A**, and **Q** tensors all coincide, the frequencies of the double-quantum transitions can be expressed as

$$\nu_{dq\pm} = \sqrt{(|A_\zeta| \pm 2\nu_n)^2 + (Q_\xi - Q_\eta)^2} \approx |A_\zeta| \pm 2\nu_n \qquad (2)$$

where Q_ξ and Q_η are the remaining principal components of the **Q** tensor. Their modulation amplitudes relative to the nonmodulating $\nu = 0$ component (per one nitrogen) can be obtained according to Flanagan and Singel[36] as

$$I(\nu_{dq\pm})/I(0) = 4k^2/3 \qquad (3)$$

for two-pulse ESEEM and

$$I(\nu_{dq\pm})/I(0) = 2k^2(1 - \cos 2\pi\, \nu_{dq\mp}\tau)/3 \qquad (4)$$

for three-pulse ESEEM, where $k = A_\zeta\,(Q_\xi - Q_\eta)/(\nu_{dq+}\nu_{dq-})$. The cosine term in eq 4 expresses the τ-suppression (or enhancement) effect. Such simple τ-suppression effects can be generally expected as long as the double-quantum transitions of the $I = 1$ system are concerned.[37] The quantity k can be reduced to $k \approx (Q_\xi - Q_\eta)/A_\zeta$ when the relation HFC ≫ NQC, NZC holds as in the VO^{2+} complexes studied here. On the other hand, under exact cancelation, where NQC ≫ |HFC − NZC|, k can be reduced to $k \approx A_\zeta/(Q_\xi - Q_\eta)$. This equation is in accordance with the previously reported tendency of the ESEEM line intensities under exact cancellation.[34] The amplitudes of the "sum and difference" combinations of the double-quantum transitions $\nu_{dd\pm} = \nu_{dq+} \pm \nu_{dq-}$ can be obtained with the same manner[36] as

$$I(\nu_{dd\pm})/I(0) = -2k^2/3 \qquad (5)$$

On the other hand, the single-quantum frequencies $\nu_{sq\pm}^{(1)}$ and $\nu_{sq\pm}^{(2)}$ can be expressed as

$$\nu_{sq\pm}^{(1)} = \nu_{dq\pm}/2 + 3|Q_\zeta|/2 \approx |A_\zeta|/2 \pm 2\nu_n + 3|Q_\zeta|/2 \qquad (6)$$

and

$$\nu_{sq\pm}^{(2)} = \nu_{dq\pm}/2 - 3|Q_\zeta|/2 \approx |A_\zeta|/2 \pm 2\nu_n - 3|Q_\zeta|/2 \qquad (7)$$

Their modulation amplitudes are exactly the zero in this simplified system. Their "sum and difference" combinations also have exactly the zero amplitude. These lines are therefore only observable when the applied field is deviated from the tensor axes, or either the **g**, **A**, or **Q** tensor axis is not collinear with others. Thus the single-quantum lines and their "sum and difference" lines can be used as an indicator of the deviation of the tensor axes. Such selection rules were first pointed out by Flanagan *et al.*[34] They showed that the quadrupole transitions, ν_0, ν_-, and ν_+, observed under exact cancelation are, in a sense, *z*, *y*, and *x* polarized, respectively. (Under exact cancelation, the double-quantum transition ν_{dq-} becomes ν_0, ν_-, and ν_+ when ζ coincides with the *z*, *y*, and *x* axis, respectively.) On this basis, the orientations of the NQC tensor axes of the imidazole nitrogen in Fe^{3+}−myoglobin−SEt were determined by ESEEM spectroscopy.[38]

It is important to note the difference between eq 2 and the well-known equation given by Astashkin *et al.*[39]

$$\nu_{dq\pm} = \sqrt{(|A| \pm 2\nu_n)^2 + 4K^2(3 + \eta^2)} \qquad (8)$$

where $K = \max\{|Q_\xi|, |Q_\eta|, |Q_\zeta|\}/2$ and η is the asymmetry factor of the NQC tensor. This equation expresses the maxima of the double-quantum frequencies in the powder spatial summation (under the constraint of isotropic HFC).[34,39] Thus this equation must be taken as designed for the case of no orientation selection. On the other hand, eq 2 is designed for the case of (strict) orientation selection. Note that eq 2 permits the anisotropy of HFC, though it assumes that the applied field and the **g**, **A**, and **Q** tensor axes coincide. Equation 8 might be also used for the case of incomplete orientation selection, which typically occurs when measurements are made at the CW EPR $g_\perp$ line. However, one must take care whether the maxima can be encountered in the *xy* summation or, more basically, whether the anisotropy of HFC is negligible compared to isotropic HFC and NQC.[40] Because of this ambiguity, we estimated only an HFC parameter in the initial analyses of the data obtained with $g_\perp$ line excitation by using[39]

$$|A_\perp| = ({\nu_{dq+}}^2 - {\nu_{dq-}}^2)/(8\nu_n) \qquad (9)$$

which follows from both eq 2 and eq 8.

Results

VO(edda). The CW EPR spectrum of VO(edda) in H_2O/ethylene glycol (1:1 v/v) glass is shown in Figure 2 as a representative of the spectra of the oxovanadium(IV) complexes studied here. The highly anisotropic HFC due to the ^{51}V nucleus

(34) Flanagan, H. L.; Singel, D. J. *J. Chem. Phys.* **1987**, *87*, 5606−5616.
(35) Reijerse, E. J.; van Aerle, N. A. J. M.; Keijzers, C. P. *J. Magn. Reson.* **1986**, *67*, 114−124.
(36) Flanagan, H. L.; Singel, D. J. *J. Phys. Chem.* **1988**, *89*, 2585−2586.
(37) Cosgrove, S. A.; Single, D. J. *J. Phys. Chem.* **1990**, *94*, 2619−2623.
(38) Flanagan, H. L.; Gerfen, G. J.; Lai, A.; Singel, D. J. *J. Chem. Phys.* **1988**, *88*, 2162−2168.
(39) Astashkin, A. V.; Dikanov, S. A.; Tsvetkov, Yu. D. *Zh. Strukt. Khim.* **1984**, *25*, 53−64.
(40) Cosgrove, S. A.; Single, D. J. *J. Phys. Chem.* **1990**, *94*, 8393−8396.

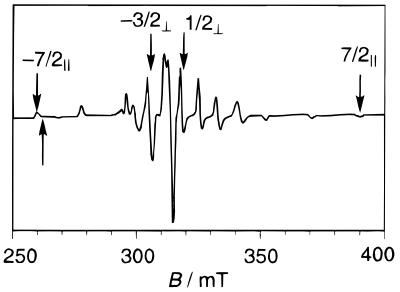

Figure 2. CW EPR spectrum of VO(edda) in H_2O/ethylene glycol (1:1 v/v) glass. The arrows indicate important peaks and the positions where ESEEM measurements were carried out (though the actual field may be slightly different due to a difference in operation frequency). Conditions: frequency, 8.843 GHz; power = 5 mW; modulation, 1 mT; temperature, 77 K.

($I = {}^7/_2$) well separates the parallel and perpendicular lines, which facilitates selective excitation of the molecules having a particular orientation about the applied field. In particular, the orientation selection would be most effective when the $m_I(^{51}V) = \pm{}^7/_2$ parallel lines and the $m_I(^{51}V) = -{}^3/_2$ and ${}^1/_2$ perpendicular lines are excited. Some of the ESEEM spectra obtained for VO(edda) are shown in Figure 3, where the selected fields are 258.2 mT ($m_I(^{51}V) = -{}^7/_2$ parallel line), 316.6 mT ($m_I(^{51}V) = {}^1/_2$ perpendicular line), and 261.2 mT (intermediate position near the $m_I(^{51}V) = -{}^7/_2$ parallel line). In the two-pulse and three-pulse ESEEM spectra recorded at the parallel line (Figure 3a,b), two intense peaks are resolved at 4.4 and 7.2 MHz. These are attributed to the ^{14}N double-quantum lines $\nu_{dq\pm}$. The separation between the two lines (2.8 MHz) is slightly but obviously small compared with the value predicted by the first-order equation, $4\nu(^{14}N)$ (=3.18 MHz under $B = 258.2$ mT), indicating significant second-order effects. We obtained $|A_z| = 5.1$ and $|Q_x - Q_y| = 2.6$ MHz by using eq 2. This $|A_z|$ value is smaller than the center frequency of $\nu_{dq\pm}$ (=5.8 MHz) by 0.7 MHz, which corresponds to the second-order correction. The two-pulse spectrum also exhibits negative-amplitude peaks at 2.7 and 11.6 MHz. These frequencies match $\nu_{dq+} - \nu_{dq-}$ and $\nu_{dq+} + \nu_{dq-}$, respectively, and thus these lines are attributed to the sum and difference lines of the double-quantum transitions, $\nu_{dd\pm}$. The appearance of $\nu_{dd\pm}$ as negative peak is in accordance with the theoretical prediction.[34,36] No clear peaks attributable to single-quantum lines are observed, which suggests that the g_z, A_z, and Q_z axes are nearly collinear.

The two-pulse and three-pulse ESEEM spectra recorded at the perpendicular line both exhibit intense lines at 3.9 and 7.2 MHz (Figures 3c,d), which are attributed to the ^{14}N double-quantum lines. Hence we estimated $|A_\perp| = 4.7$ MHz using eq 9, where $A_\perp$ denotes some average of the **A** tensor components in the *xy* plane. The two-pulse spectrum contains a negative peak at 5.7 MHz. This peak is attributed to the special sum of single-quantum lines, $\nu_{ss+} = \nu_{sq+}{}^{(1)} + \nu_{sq-}{}^{(2)}$ and $\nu_{sq-}{}^{(2)} + \nu_{sq+}{}^{(1)}$, both of which become $|A_\perp|$ in the first order. When the **A** tensor is nearly isotropic, the ν_{ss+} line is expected to be observed as a sharp line in the two-pulse spectrum even though the parent single-quantum lines may be severely broadened.[16] The observed frequency 5.7 MHz well agrees with the average $(\nu_{dq+} + \nu_{dq-})/2 = 5.55$ MHz, as expected from eqs 6 and 7, $\nu_{sq+}{}^{(1)} + \nu_{sq-}{}^{(2)} = \nu_{sq-}{}^{(2)} + \nu_{sq+}{}^{(1)} = (\nu_{dq+} + \nu_{dq-})/2$. A shoulderlike peak is additionally observed at 3.5 MHz in the three-pulse spectrum. At present the origin of this peak is not clear.

Computer simulations were performed by use of the above estimated HFC and NQC parameters as first input. The two sets of Euler angles (α_A, β_A, γ_A) and (α_Q, β_Q, γ_Q) are first set equal. Since the two amine nitrogens in VO(edda) are coordinated equatorially in *cis* positions and the g_z axis most likely coincides with the V=O bond direction, the first choice was (α_A, β_A, γ_A) = (α_Q, β_Q, γ_Q) = (0°, 90°, 0°) for one nitrogen and (90°, 90°, 0°) for the other nitrogen. Figure 4 depicts some simulated three-pulse ESEEM patterns and their cosine FFT spectra for $B||z$ computed with variation of $|Q_Y - Q_Z|$ (=$|Q_x - Q_y|$ in the **g**-tensor frame). The simulations demonstrate that the modulation depth becomes steeper as $|Q_Y - Q_Z|$ increases, which is in accordance with eq 4. The modulation depth matches with that of the experimental data at $|Q_Y - Q_Z| \sim 2.7$ MHz, which is in good agreement with $|Q_x - Q_y| = 2.6$ MHz estimated from eq 2. Having estimated $|Q_Y - Q_Z|$, we have only one NQC parameter, Q_X, to be estimated because the **Q** tensor is traceless. The absence of the single-quantum lines in the spectra recorded at the parallel line makes it impossible to estimate Q_X from these spectra. We alternatively simulated the spectrum recorded at 261.2 mT, an intermediate field close to the $m_I(^{51}V) = -{}^7/_2$ parallel line (Figure 3e). The peak at 3.1 MHz corresponds to a single-quantum line which gains intensity because of the deviation of the applied field from the tensor axes. Since the selected field is near the parallel line, simulated spectra are almost independent of A_Y and A_Z. This property allowed us to estimate Q_X efficiently (a rough estimate is $|Q_X| = 0.33$ MHz). The remaining parameters A_Y and A_Z, first set to $|A_\perp| = 4.7$ MHz, were estimated from the simulations of the spectra at the perpendicular field by a trial-and-error procedure. Having reached the best fits with the constraint of coaxial tensor

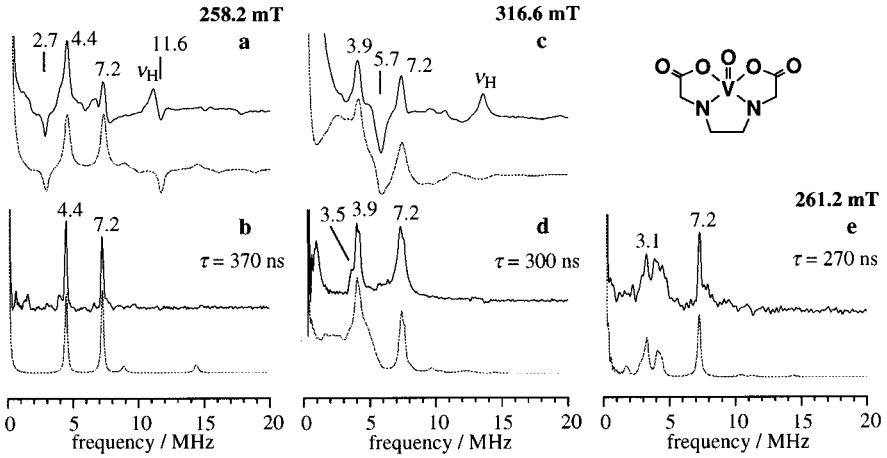

Figure 3. ESEEM spectra of VO(edda) in H_2O/ethylene glycol (1:1 v/v) glass (frequency = 8.800 GHz). The dotted lines correspond to simulations. The symbol ν_H indicates the peak due to ^{1}H nuclei. Key: (a) two-pulse spectrum at 258.2 mT.; (b) three-pulse ($\tau = 370$ ns) spectrum at 258.2 mT; (c) two-pulse spectrum at 316.6 mT; (d) three-pulse ($\tau = 300$ ns) spectrum at 316.6 mT; (e) three-pulse ($\tau = 270$ ns) spectrum at 261.2 mT.

Table 1. Hyperfine Coupling and Nuclear Quadrupole Coupling Parameters of Nitrogen-Coordinated Oxovanadium(IV) Complexes as Determined from Computer Simulation of ESEEM Data

	N^a	$\|A_X\|$ ($\approx\|A_{zz}\|$), $\|A_Y\|$,$\|A_Z\|$/ MHz (±0.05)[b]	α_A, β_A, γ_A/ deg[c]	$Q_X(\approx Q_{zz})$, Q_Y,Q_Z/ MHz (±0.1)[b]	α_Q, β_Q, γ_Q/ deg (±5)[b]	e^2qQ^g/ MHz	η^g
VO(edda)	2	5.10, 5.10, 4.75	0, 90, 0; 90, 90, 0	∓0.4, ∓1.15, ±1.55	25, 90, 0; 65, 90, 0	3.1	0.48
$VO(gly)_2$	2	5.40, 5.20, 4.70	0, 90, 10; 180, 90, 10[d] 0, 90, 10; 90, 90, 10[e]	∓1.0, ±1.35, ∓0.35	15, 90, 10; 165, 90, 10[d] 15, 90, 10; 75, 90, 10[e]	2.7	0.48
VO(salen)	2	6.30, 5.90, 5.30	0, 90, 0; 90, 90, 0	∓0.4, ∓0.8, ±1.20	*f*	2.4	0.33
VO(salophen)	2	6.30, 5.85, 5.20	0, 100, 0; 90, 100, 0	∓0.4, ∓0.9, ±1.30	*f*	2.6	0.38
$VO(NCS)_4^{2-}$	4	7.90, 7.90, 6.60	0, 90, 0; 90, 90, 0 180, 90, 0; 270, 90, 0	∓0.25, ∓0.25, ±0.5	*f*	1.0	0

[a] Number of coordinated nitrogens. [b] The numbers in the parentheses indicate respective uncertainties. [c] The uncertainty cannot be estimated because simulations are insensitive to these parameters. [d] *trans* configuration assumed. [e] *cis* configuration assumed. [f] Coaxial with the **A** tensor. [g] Calculated from Q_X, Q_Y, and Q_Z.

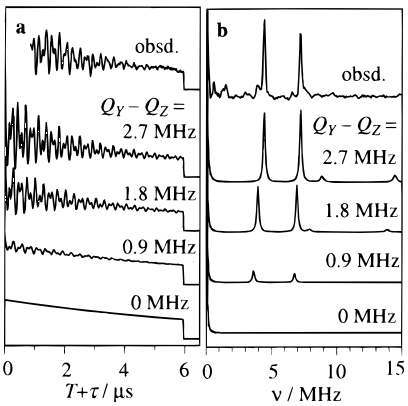

Figure 4. Experimental and some computed ESEEM patterns (a) and their spectra (b) for VO(edda) (three pulse, $\tau = 370$ ns, $B = 258.2$ mT). The computed patterns and spectra are obtained with $|Q_Y - Q_Z| = 0$, 0.9, 1.8 and 2.7 MHz and the other parameters fixed at the values listed in Table 1. In panel a, sudden drops are added at the end of the ESEEM patterns to indicate respective zero levels. Experimental data for $T + \tau > 6$ μs are omitted, and the sudden drop is only for presentation purposes.

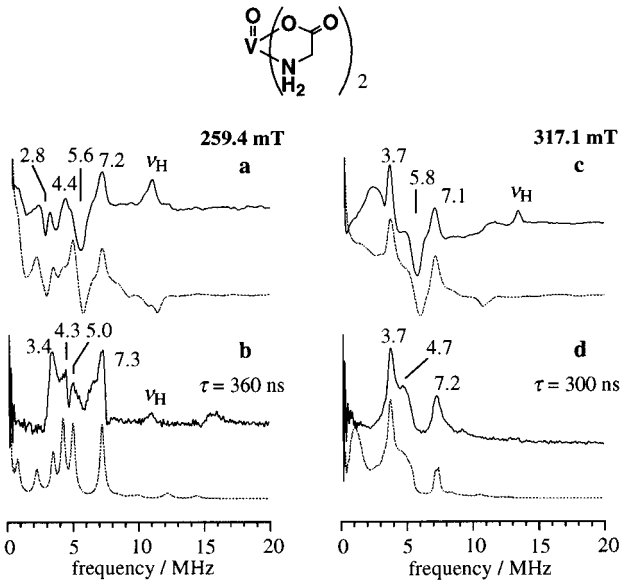

Figure 5. ESEEM spectra of $VO(gly)_2$ in H_2O/ethylene glycol (1:1 v/v) glass (frequency = 8.802 GHz). The dotted lines correspond to simulations. The symbol ν_H indicates the peak due to ^1H nuclei. Key: (a) two-pulse spectrum at 259.4 mT; (b) three-pulse ($\tau = 360$ ns) spectrum at 259.4 mT; (c) two-pulse spectrum at 317.1 mT; (d) three-pulse ($\tau = 300$ ns) spectrum at 317.1 mT.

systems, we allowed the tensor axes to misalign. It was found that variation of α_Q, in-plane rotation of the **Q** tensor frame, effectively improves the fittings. The variation of the other Euler angles did not improve the fittings. In fact, to reproduce the absence of the single-quantum lines in the spectra at the parallel line, the A_X and Q_X axes must be kept parallel or almost parallel to the g_z axis; i.e. β_A, γ_A, β_Q, and γ_Q must be kept close to their initial values. Furthermore, the **A** tensor is found to be well isotropic, so that the variation of the **A** tensor frame gives little effect. Repetitive fitting procedure has finally yielded the best fits shown in Figures 3, and the final parameters are listed in Table 1. The resulting value of $|Q_X|$ ($=|Q_z|$) = 0.4 MHz predicts the single-quantum frequencies for the parallel-line excitation as 1.6, 2.8, 3.0, and 4.2 MHz. Thus the very weak features around 1.5 and 4.0 MHz in Figure 3b may be attributed to single-quantum lines. (The simulation in Figure 3b also contains very weak peaks at 8.8 and 14.4 MHz. These are due to combination harmonics, $2\nu_{dq-}$ and $2\nu_{dq+}$, appearing because of multiple nitrogens.)[32]

$VO(gly)_2$. Tipton *et al.*[15] previously reported ESEEM results of this complex. However, they reported only the spectra recorded at the $m_I(^{51}V) = -1/2$ line, though with two frequency settings 8.826 and 10.125 GHz. Thus the reported HFC and NQC parameters may have ambiguity (actually $A_{xx} = A_{yy}$ in their simulation). Because of the relevance of $VO(gly)_2$ to biological systems, we re-investigated this complex. Figure 5 shows two-pulse and three-pulse ESEEM spectra of $VO(gly)_2$ in H_2O/ethylene glycol (1:1 v/v) glass, where the selected fields are 259.4 mT ($m_I(^{51}V) = -7/2$ parallel line) and 317.1 mT ($m_I(^{51}V) = 1/2$ perpendicular line). The two-pulse and three-pulse ESEEM spectra at the parallel line (Figures 5a,b) have a complicated pattern compared with the corresponding spectra of $VO(edda)_2$. The peaks at 4.4 and 7.2 MHz in the two-pulse spectrum and the peaks at 4.3 and 7.3 MHz in the three-pulse spectrum have a separation comparable to $4\nu(^{14}N)$ and, thus, are assigned to the double-quantum lines. From the frequencies in the three-pulse spectrum we estimated $|A_z| = 5.4$ and $|Q_x - Q_y| = 1.9$ MHz. It seems that the peaks at 3.4 and 5.0 MHz in the three-pulse spectrum correspond to the feature at 3.2 MHz and the shoulder near 5.0 MHz in the two-pulse spectrum (not indicated in the figure), respectively. Their separation is too small to assign to the double-quantum lines. These peaks can be attributed to single-quantum lines appearing because of a deviation of the A_z and/or Q_z axes from the g_z axis. Assignments of the higher frequency peak to $\nu_{sq+}^{(1)}$ and the lower frequency peak to $\nu_{sq-}^{(1)}$ give a consistent estimate of $|Q_z| = 0.8-0.9$ MHz. The negative peaks at 2.8 and 5.6 MHz in the two-pulse spectrum are reasonably assigned to ν_{dd-} and ν_{ss+}, respectively. The appearance of the latter line ν_{ss+} in the spectrum obtained with parallel-field setting also indicates a misalignment of the tensor axes. The two-pulse and three-pulse spectra recorded at the perpendicular line (Figures 5c,d) are rather featureless compared with the spectra at the parallel line. The 3.7 and 7.1 MHz peaks in the two-pulse spectrum and the 3.7 and 7.2 MHz peaks in the three-pulse spectrum are assigned to the double-

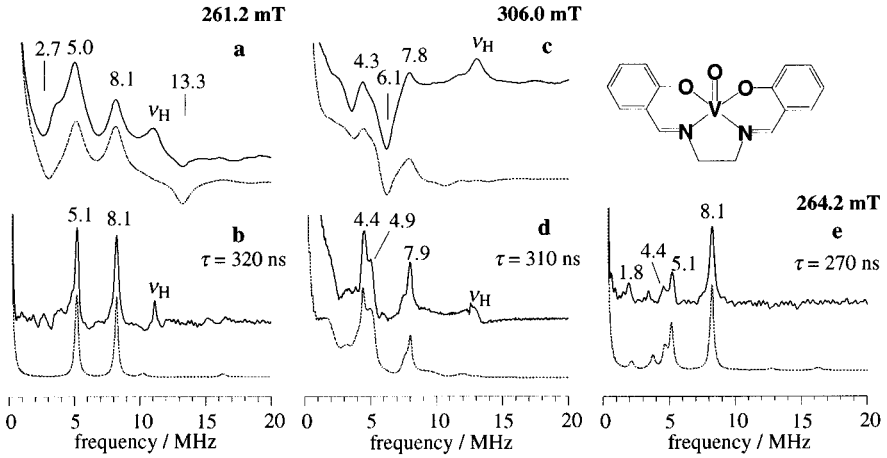

Figure 6. ESEEM spectra of VO(salen) in DMF/toluene (1:1 v/v) glass (frequency = 8.806 GHz). The dotted lines correspond to simulations. The symbol ν_H indicates the peak due to ^{1}H nuclei. Key: (a) two-pulse spectrum at 261.2 mT; (b) three-pulse (τ = 320 ns) spectrum at 261.2 mT; (c) two-pulse spectrum at 306.0 mT; (d) three-pulse (τ = 310 ns) spectrum at 306.0 mT; (e) three-pulse (τ = 270 ns) spectrum at 264.2 mT.

quantum lines ($|A_\perp|$ = 4.9 MHz from the three-pulse spectrum). The negative peak at 5.8 MHz in the two-pulse spectrum is assigned to ν_{ss+}.

While the two amine nitrogens in VO(gly)$_2$ are very likely coordinated equatorially, it is not known whether the nitrogens are in *cis* conformation or *trans* conformation. Thus the simulations were performed for two conformations. For *cis* conformation, the Euler angles were first set as (α_A, β_A, γ_A) = (α_Q, β_Q, γ_Q) = (0°, 90°, 0°) for one nitrogen and (90°, 90°, 0°) for the other. For *trans* conformation, on the other hand, the first choice was (α_A, β_A, γ_A) = (α_Q, β_Q, γ_Q) = (0°, 90°, 0°) and (180°, 90°, 0°) for the two nitrogens. As noted in the Theoretical Background section, the nonzero intensities of the single-quantum lines in the spectra recorded with the parallel-field setting could not be reproduced with these first sets of Euler angles. It was found that the angle responsible for this is γ_Q, corresponding visually to the rotation about the V−N bond direction. With the increase of γ_Q from 0°, the single-quantum lines become visible through reasonable reproduction of the experimental data around 10° and become too intense at $\gamma_Q \sim 15°$. (Table 1 includes γ_A = 10° as well as γ_Q. This is because we set the **A** and **Q** tensors coaxial in the initial stage of the simulation. As a matter of fact, the rotation of the **A** tensor frame has little effect owing to the isotropic nature of HFC, so that we were unable to determine γ_A and have left γ_A at the value of the initial stage.) In the variation of γ_Q, however, the 5.0 MHz peak was always more intense than the 3.4 MHz peak, so that we were unable to fit the intensity distribution of the single-quantum lines completely. The variation of the other parameters also failed to reproduce this intensity distribution. This disagreement is presumably because the two nitrogens are not ideally symmetry-related and/or there is heterogeneity in the complex geometry and the nitrogen HFC and NQC parameters, both of which were not included in the simulation. It was also found that, in the simulation of the three-pulse spectrum at the perpendicular line (Figure 5d), the variation of α_Q improves the fitting to the line shapes of the 3.7 MHz peak and the 4.7 MHz shoulder. The best fits were achieved when $\alpha_Q = \alpha_A \pm 15°$ for both the two conformations. Satisfactory fits were finally obtained for the two conformations. Of the two conformations, *trans* conformation provided slightly better fits than *cis* conformation. The simulated spectra presented in Figure 5 are those obtained for *trans* conformation. We however note that the differences between the simulated ESEEM patterns for the two conformations are too slight to allow convincing determination of the actual conformation. In fact, the differences are only about the "multinuclear" combination harmonics, which can depend on the relative position of the two nitrogens. More detailed and specially designed experiments would be required if one aims to decide the actual conformation by ESEEM spectroscopy.

Tipton *et al.*[15] reported three-pulse ESEEM spectra of VO(gly)$_2$ recorded at two different frequencies but with excitation of the same $m_I(^{51}V) = -1/2$ line. The parallel and perpendicular lines overlap at the $m_I(^{51}V) = -1/2$ line, so that no orientation selection was made in their experiments. From the simulation, they obtained $A_{zz} = A_{yy} = 4.85$, $A_{zz} = 5.3$, $e^2qQ = 2.55$ MHz, and $\eta = 0.5$. Now we can compare our results with theirs. In our simulation, the *X* axis is approximately parallel to the molecular *z* axis and the *Y* and *Z* axes fairly lie in the molecular *xy* plane. Thus our results can be converted into A_{xx} (=A_{yy}) and A_{zz} with the eqs $(A_Y + A_Z)/2 = A_{xx}$ and $A_X = A_{zz}$, which provide $A_{xx} = 4.95$ MHz and $A_{zz} = 5.4$ MHz. These values are in excellent agreement with the values reported by Tipton *et al*. As for the NQC parameters, e^2qQ is the double of the **Q** principal value having the largest magnitude. Thus our results correspond to $e^2qQ = 2Q_Y = 2.7$ MHz and $\eta = (Q_X - Q_Z)/Q_Y = 0.48$ (Table 1), which are also in good agreement with theirs.

VO(salen) and VO(salophen). The results for VO(salen) and VO(salophen) are quite similar, so that we describe the results together. The CW EPR spectra of VO(salen) and VO(salophen) in DMF/toluene (1:1 v/v) glass exhibited slight rhombicity with higher-field perpendicular lines split into their *x* and *y* components.[41] Nevertheless, while the splitting is most noticeable at the highest-field $m_I(^{51}V) = 7/2$ line, the splitting becomes smaller as the resonant field decreases and eventually becomes unresolved below the $m_I(^{51}V) = 1/2$ line. At the region of the $m_I(^{51}V) = -3/2$ line, at which ESEEM measurements were made, no evidence of rhombic splitting was observed (peak-to-peak width $\approx$ 1 mT). Therefore the effects of the **g** rhombicity can be ignored in the following ESEEM results.

Figure 6 presents ESEEM spectra of VO(salen) recorded at 261.2 mT ($m_I(^{51}V) = -7/2$ parallel line), 306.0 mT ($m_I(^{51}V) = -3/2$ perpendicular line), and 264.2 mT (intermediate position close to the $m_I(^{51}V) = -7/2$ parallel line). These spectra can be interpreted in the same manner as described above. The two-pulse spectrum in Figure 6a exhibits the double-quantum lines at 5.0 and 8.1 MHz and their sum and difference lines $\nu_{dd\pm}$ at 2.7 and 13.3 MHz. The 2.7 MHz peak is slightly distorted, and thus its frequency is not in good agreement with

(41) Jezerski, A.; Raynor, J. B. *J. Chem. Soc., Dalton Trans.* **1981**, 1−7.

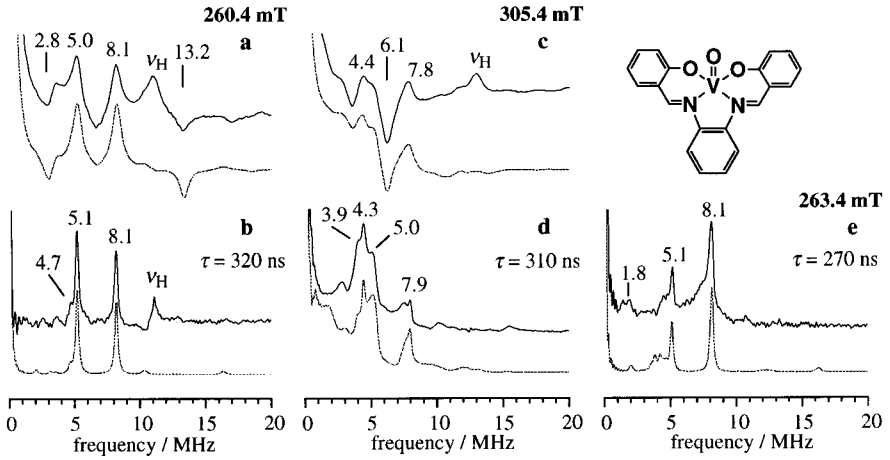

Figure 7. ESEEM spectra of VO(salophen) in DMF/toluene (1:1 v/v) glass (frequency = 8.811 GHz). The dotted lines correspond to simulations. The symbol ν_H indicates the peak due to ^{1}H nuclei. Key: (a) two-pulse spectrum at 260.4 mT; (b) three-pulse (τ = 320 ns) spectrum at 260.4 mT; (c) two-pulse spectrum at 305.4 mT; (d) three-pulse (τ = 310 ns) spectrum at 305.4 mT; (e) three-pulse (τ = 270 ns) spectrum at 263.4 mT.

the difference $\nu_{dq+} - \nu_{dq-}$. This slight disagreement and the presence of an edge feature at ~3.5 MHz suggest an unresolved peak near this frequency. The three-pulse spectrum in Figure 6b shows the double-quantum lines at 5.1 and 8.1 MHz, which gives $|A_z| = 6.2$ MHz and $|Q_x - Q_y| = 2.3$ MHz. With the perpendicular field setting, the two-pulse spectrum exhibits the double-quantum lines at 4.3 and 7.8 MHz and the ν_{ss+} line at 6.1 MHz (Figure 6c). The three-pulse spectrum recorded with the same field setting exhibits the double-quantum lines at 4.4 and 7.9 MHz ($|A_\perp| = 6.2$ MHz) and a shoulder at 4.9 MHz due to the high-frequency edge of a single-quantum line[18,19] (Figure 6d). In the spectrum recorded at the intermediate field, two single-quantum lines are well resolved at 1.8 and 4.4 MHz as well as the double-quantum lines at 5.1 and 8.1 MHz (Figure 6e). The two single-quantum lines are assigned to $\nu_{sq+}^{(1)}$ and $\nu_{sq-}^{(2)}$, which gives an estimate of $|Q_z| = 0.37 \pm 0.13$ MHz from eqs 6 and 7. This estimate predicts that the remaining two single-quantum frequencies are ca. 3.1 and 3.5 MHz. Thus the weak feature around 3.5 MHz may be assigned as a single-quantum line.

Figure 7 shows the ESEEM spectra of VO(salophen) recorded with the same field settings as for VO(salen) (though the actual fields are slightly different). These spectra are quite similar to the corresponding ones of VO(salen). Slight but important differences are however observed: In the two-pulse spectrum recorded at the parallel line (Figure 7a), the edge feature around 3.5 MHz is more obvious than in the corresponding spectrum of VO(salen). In addition, the feature between the 5.0 and 8.1 MHz peaks drops more steeply in the spectrum of VO(salophen), suggesting the presence of an unresolved negative peak between them. The three-pulse spectrum recorded at the parallel line (Figure 7b) exhibits a shoulder at 4.7 MHz. A new shoulder also appears at 3.9 MHz in the three-pulse spectrum recorded at the perpendicular lines (Figure 7d).

Computer simulations for the spectra of VO(salen) and VO(salophen) were conducted with the same procedure described above. The computer simulations have revealed that the differences between the spectra of the two complexes are due essentially to a tilt of the Q_z axis in VO(salophen). Simulations with β_Q ($=\beta_A$) ~ 10° well reproduced the features in VO(salophen) while satisfactory fits were obtained with β_Q ($=\beta_A$) ~ 0° for VO(salen). Variation of the other Euler angles did not improve the fittings: For example, variation of α_Q, which is successful in the cases of VO(edda) and VO(gly)$_2$, only makes the 4.4 MHz peak (Figure 6d) broad and merged with the 4.9 MHz shoulder. The final parameters obtained are included in Table 1. For VO(salen), the slight disagreement between the experimental and simulated spectra about the edge feature (Figure 6a) suggests a slight misalignment of the tensor axes. However, although the fit to this spectrum was indeed improved by slight variation of β_Q, the fits to the other spectra became poor. Variation of the other Euler angles also did not improve the total fittings. We have therefore left the **g**, **A**, and **Q** tensors coaxial.

With the help of the computer simulation, we can make further assignments with respect to the features observed for VO(salophen). According to the simulation, the edge feature around 3.5 MHz is due to the single-quantum lines $\nu_{sq-}^{(1)}$ and $\nu_{sq+}^{(2)}$ distorted by the overlap with ν_{dd-}. These single-quantum lines appear because of the misalignment of the tensor axes. The simulation also predicts the appearance of ν_{ss+} at 6.7 MHz as a negative peak with the tilt of the Q_z axis, which accounts for the steep drop between the 5.0 and 8.1 MHz lines (Figure 7a). The 4.7 MHz shoulder in Figure 7b is assigned to the single-quantum line $\nu_{sq+}^{(1)}$ on the basis of the simulation. The 3.9 MHz shoulder in Figure 7d is assigned to the lower-frequency partner of the double-quantum lines corresponding to a different stationary direction from that of the 4.3 and 7.9 MHz pair (see Discussion).

VO(NCS)$_4$. The two-pulse ESEEM spectrum of VO(NCS)$_4^{2-}$ in MeOH/ethylene glycol (3:1) glass recorded at the lowest-field parallel line ($m_I(^{51}V) = -^7/_2$) is shown in Figure 8a. The echo modulation due to the isothiocyanate ^{14}N nuclei was found to be quite shallow, and thus the presented spectrum is noisy. Only one peak at 6.4 MHz is clearly resolved in the spectrum. The ESEEM pattern recorded at another parallel line ($m_I(^{51}V) = ^7/_2$) was also shallow, yet its spectrum resolves two peaks at 5.6 and 10.3 MHz (Figure 8b). The field dependence of 6.4 → 5.6 MHz with B = 259.0 → 387.6 mT is consistent with the expected behavior of ν_{dq-}. Thus we assign the 6.4 MHz peak in Figure 8a and the 5.6 and 10.3 MHz peaks in Figure 8b to the double-quantum lines ($|A_z| \approx 7.8$ MHz). The partner of the 6.4 MHz peak in Figure 8a is expected to appear at 9.5 MHz. In the observed spectrum, the 9.5 MHz peak is almost buried under the tail of the ^{1}H peak. We also performed three-pulse ESEEM measurements at the two parallel lines. However, the echo modulations were extremely shallow so that no peaks were resolved in the FT spectra despite that the echo height itself was sufficiently strong. The ESEEM spectra recorded at 303.3 mT ($m_I(^{51}V) = -^3/_2$ perpendicular line) exhibit a different pattern from those of the other complexes. The two-pulse spectrum contains well-resolved peaks at 2.8 and 4.8 MHz

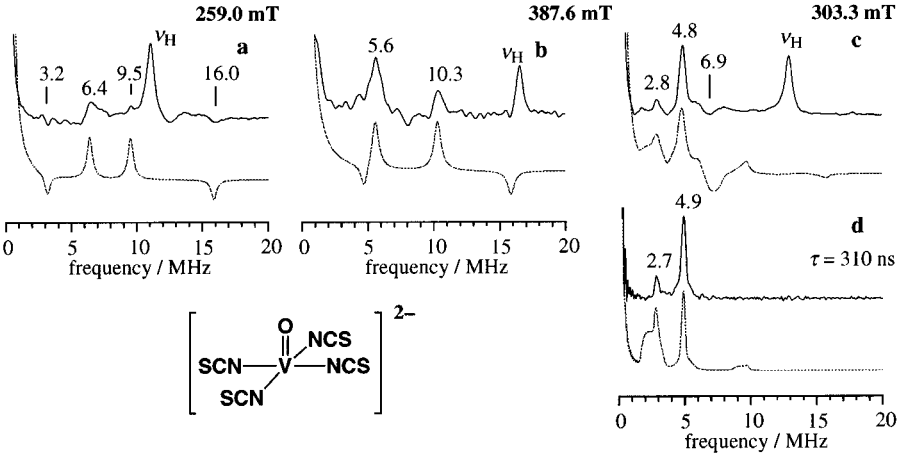

Figure 8. ESEEM spectra of $VO(NCS)_4^{2-}$ in MeOH/ethylene glycol (3:1 v/v) glass (frequency = 8.802 GHz). The dotted lines correspond to simulations. The symbol ν_H indicates the peak due to ^{1}H nuclei. Key: (a) two-pulse spectrum at 259.0 mT; (b) two-pulse spectrum at 387.6 mT; (c) two-pulse spectrum at 303.3 mT; (d) three-pulse (τ = 310 ns) spectrum at 303.3 mT.

(Figure 8c), and the three-pulse spectrum also exhibits peaks at practically the same frequencies 2.7 and 4.9 MHz (Figure 8d). It seems impossible to interpret these spectra without computer simulation.

Since the experimental data do not contain sufficient information for determination of the many parameters in the simulation, we placed some restrictions on the simulation parameters: The **g**, **A**, and **Q** tensors are set coaxial, and the **A** and **Q** tensors are assumed to be uniaxial with respect to the V−N direction. These constraints are based on the X-ray data showing that the NCS^- ligands are well placed in the equatorial plane and the atoms V−N−C−S align linearly.[30] The peak frequencies and the modulation amplitudes of the ESEEM data recorded at the parallel lines are well reproduced with $|A_z| = 7.9$ MHz, and $|Q_x - Q_y| = 0.75$ MHz. Since the **A** and **Q** tensors are assumed uniaxial, they immediately give $|A_X| = |A_Y| = 7.9$ MHz, $Q_X = Q_Y = \pm 0.25$ MHz, and $Q_Z = \mp 0.50$ MHz (the *Z* axis is set parallel to the V−N direction, and the *X* axis parallel to the molecular *z* axis). The resulting NQC parameters agree well with the previous NQR results ($e^2qQ = 2Q_Z = 0.947$, 0.887 MHz and $\eta = 0.211$, 0.224 for $Zn(pyridine)_2(NCS)_2$).[42] The remaining parameter A_Z was varied to achieve fits to the spectra recorded at the perpendicular lines. The above procedure was repeated to refine the HFC and NQC parameters, and the parameters listed in Table 1 were finally obtained.

The resulting e^2qQ value is quite small compared with those of the other complexes, which can be attributed to the extremely shallow modulations. The expected modulation amplitude per one nitrogen for the g_z line excitation ($B||A_X, Q_X$), for instance, is proportional to $k^2 \approx |Q_Y - Q_Z|^2/|A_X|^2$ (eq 3) From the resulting HFC and NQC parameters, we can estimate $k^2 \approx 5 \times 10^{-3}$. This value is much smaller than the k^2 values of VO(edda) ($k^2 \approx 3 \times 10^{-1}$) and VO(salen) ($k^2 \approx 1$ x 10^{-1}) estimated similarly from their HFC and NQC parameters.

From comparison with the simulations, the dips at 3.2 and 16.0 MHz in Figure 8a are assigned to the sum and difference lines $\nu_{dd\pm}$, and the broad dip at 6.9 MHz in Figure 8c is assigned to ν_{ss+}. Interpretation of the other peaks in Figures 8c,d is discussed in the next section.

Discussion

From the computer simulation, we have determined the HFC **A** and NQC **Q** tensors (principal values and principal-axis orientations) of the coordinated ^{14}N nuclei in the five oxovanadium(IV) complexes (Table 1). Although the *Y* and *Z* axes are experimentally indistinguishable, we have assigned the axis containing the smallest magnitude of **A** component to the *Z* axis (the component along the V−N bond direction),[19] which will be supported by the consideration on the mechanism of HFC (*vide infra*). Additionally, the NQC axis parallel or most parallel to A_Z is assigned to Q_Z. In the simulation, we set the **A** and **Q** tensors coaxial unless to change this is necessary to provide better fits. As a matter of fact, computed ESEEM patterns and their spectra were usually insensitive to the variation of the **A** tensor Euler angles owing to the well isotropic nature of the **A** tensor. In the case of VO(salophen), for example, equally good fits were obtained with $\beta_A = 90°$ instead of $\beta_A = 100°$ (with β_Q fixed at 100°). It seems almost impossible to determine the **A** tensor orientations precisely for these complexes. In contrast, computed results were sensitive to the **Q** tensor Euler angles, and we were able to determine the **Q** tensor orientations enough reliably.

The ESEEM spectra recorded with the parallel-field settings were quite informative, allowing immediate estimates of $|A_z|$ and $|Q_x - Q_y|$ from the double-quantum frequencies. Some of the spectra also contain single-quantum lines, which also enabled us to estimate $|Q_z|$ immediately. Furthermore, the intensities of the single-quantum lines provided insights into the deviation of the **Q** tensor axes from the **g** tensor axes. When the single-quantum lines were not resolved in the spectra, we estimated $|Q_z|$ from the spectra recorded at an intermediate field near the parallel line. This approach will be widely applicable to interpret ESEEM data of the strong HFC condition.

On the other hand, analyzing the ESEEM spectra recorded with the perpendicular-field settings was not straightforward. It seems that $|A_\perp|$ is the only parameter that one can estimate immediately. To gain further insights into these spectra, we examined the angular dependence of the three-pulse ESEEM frequencies and intensities computed using the parameters obtained from the simulations. The results computed for three representative complexes, VO(edda), VO(salophen) and $VO(NCS)_4^{2-}$, are shown as contour plots in Figure 9. In the plots only the fundamental lines of one nitrogen are shown for clarity. The applied field is rotated within the *xy* plane, being parallel or most parallel to the A_Z axis (visually corresponding to the V−N bond direction) at 0° and parallel to the A_Y axis at 90°. Figure 9a shows the contour plot computed for the three-pulse ESEEM lines of VO(edda). The traces varying around 7 MHz

(42) Hsieh, Y.-N.; Rubenacker, G. V.; Chemg. C. P.; Brown, T. L. *J. Am. Chem. Soc.* **1977**, *99*, 1384−1389.

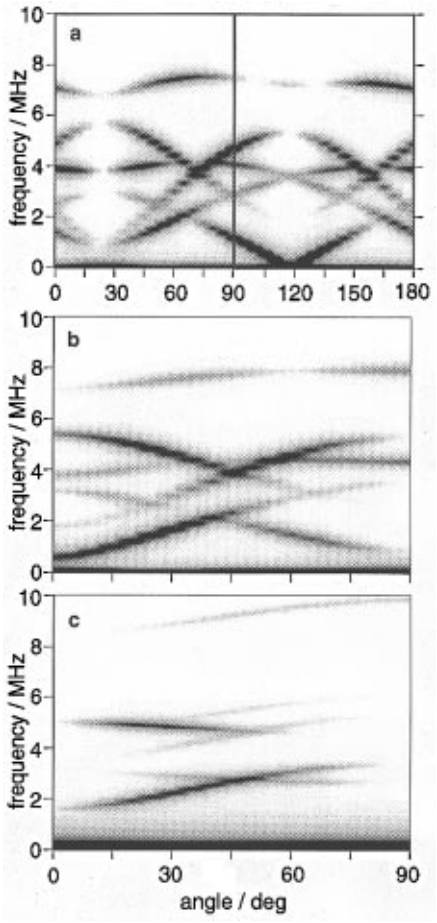

Figure 9. Contour plots showing the variations of the positions and intensities of the three-pulse ESEEM lines with the direction of the applied field. The ESEEM lines from only one nitrogen are shown for clarity. The applied field is parallel or most parallel to the A_Z axis at 0° and parallel to the A_Y axis at 90°. The plots are computed with the parameters obtained for (a) VO(edda), (b) VO(salophen), and (c) $VO(NCS)_4^{2-}$. See Table 1 for the parameters.

and 3.5−4 MHz correspond to the double-quantum lines ν_{dq+} and ν_{dq-}, respectively, and the other traces to the single-quantum lines. According to the simulation, the A_Z and Q_Z axes and the A_Y and Q_Y axes are not collinear in this complex with the deviation angle being 25°. The applied field is therefore parallel to the Q_Z and Q_Y axes at 25 and 115°, respectively. The plot shows that the stationary points of the ESEEM lines rather appear at these angles. The single-quantum lines exhibit their minimum intensities at these angles. This is because, as noted in the Theoretical Background section, the single-quantum lines should disappear when all the relevant orientations coincide. For VO(edda), the **g** tensor is axial and the **A** tensor is nearly isotropic, so that only the orientations of applied field and the **Q** tensor axes are relevant to the *xy*-plane variation. When the applied field is off the stationary points, on the other hand, the single-quantum lines have considerable intensities. In spite of this, however, since their line positions show vigorous angular dependence, the summation of these lines over the *xy* plane results in only broad backgroundlike features. In contrast, the positions of the double-quantum lines are much less dependent on the direction of the applied field, and eventually only these lines form resolved peaks in the spectrum.[34] Quite interestingly, the frequencies and intensities of the double-quantum lines show anomalous angular dependence owing to the misalignment between the HFC and NQC axes. This accounts for the small splittings of the 3.9 and 7.2 MHz peaks in the experimental spectrum (Figure 3d). Inspection of the plots also reveals that the 3.5 MHz shoulder comes from the ν_{dq-} line at a stationary point of 115°.

The contour plot in Figure 9b shows the angular dependence of the three-pulse ESEEM lines of VO(salophen). The traces varying around 7−8 MHz and around 4 MHz correspond to the ν_{dq+} and ν_{dq-} lines, respectively, and the other traces to the single-quantum lines. According to the simulation, the HFC and NQC axes are collinear in this complex, but they are not coincident with the **g** axes; i.e. the A_Z and Q_Z axes are tilted by 10° from the *xy* plane. Thus the applied field is not parallel to the A_Z or Q_Z axes at 0°, and the single-quantum lines have nonzero intensities at this angle. In particular, the single-quantum line situated at 5.4 MHz at 0° exhibits a considerable intensity around this angle. Thus the 5.0 MHz shoulder in the experimental spectrum (Figure 7d) can be attributed to this line. The disagreement between the frequencies in the contour plot (5.4 MHz at 0°) and in the spectrum (5.0 MHz) should be noted. This is partly because of the overlap with another single-quantum line, which is situated at 5.3 MHz at 90°. Moreover it is essentially due to the somewhat perverse behavior of the intensity of the single-quantum line. The intensity shows its maximum off the stationary point, and as the angle approaches the stationary point, the intensity decreases and reaches its local minimum at the stationary point. As a result of this, the peak frequency in the *xy* summed spectrum does not match the frequency at the stationary point. Rather the tail end of the peak seems to well correspond to the frequency at the stationary point. Another important insight into the experimental spectrum can be gained concerning the assignment of the 3.9 MHz shoulder. In the plot, the lower-frequency partner of the double-quantum line ν_{dq-} is situated at 3.8 MHz at 0° with an appreciable intensity. Thus the 3.9 MHz shoulder in the experimental spectrum is assigned to the 0° component of the ν_{dq-} line. Quite interestingly, this shoulder does not appear in the corresponding spectrum of VO(salen) (Figure 6d). This can be explained as follows: According to the computer simulation, the essential difference between VO(salen) and VO(salophen) is that the **g**, **A**, and **Q** tensors are well coaxial in VO(salen) while the **A** and **Q** tensor frames are slightly tilted from the **g** tensor frame in VO(salophen). For VO(salen), therefore, eq 4 can be applied when the applied field is parallel to the *Z* and *Y* axis. According to eq 4, the intensities of the double-quantum lines are expected to be proportional to $k^2 \approx |(Q_X - Q_Y)/A_Z|^2 = 6 \times 10^{-3}$ at 0° ($B||Z$) and $k^2 \approx |(Q_X - Q_Z)/A_Y|^2 = 7 \times 10^{-2}$ at 90° ($B||Y$). Comparison between the two values shows that the intensity at 0° are much weaker than the intensity at 90°, explaining the absence of the 0° component in Figure 6d. In VO(salophen), on the other hand, the Q_Z axis is deviated from the g_x axis. Then the 0° component will be more intense because the deviation of the applied field from the NQC axis allows further mixing of the states. This explains the appearance of the 0° component in Figure 7d. In the contour plot, the angular dependence of ν_{dq+} is also worth noting. This line shows considerable intensities in two separate regions, 15−45° and 75−90°. This accounts for the unique shape of the ν_{dq+} line, which consists of the sharp peak at 7.9 MHz and the broad feature around 7.5 MHz (Figures 6d and 7d). The contributions from 15−45° and 75−90° must correspond to the broad feature around 7 MHz and the sharp feature at 7.9 MHz, respectively.

For $VO(NCS)_4$, only a few lines are seen in the contour plot (Figure 9c). As noted in Results section, the double-quantum lines are not observed because of the relatively small NQC and large HFC. In the plot, only a faint trace is seen near 10 MHz around 90°. The peak corresponding to this trace is, of course, not resolved in the experimental spectrum (Figure 8d). Of the

traces concerning the single-quantum lines, three traces exhibit appreciable intensities. One trace becomes visible around 5 MHz when the angle is 10−50°. This trace must correspond to the 4.9 MHz peak in the experimental spectrum. Since the frequency of this trace varies very gradually, this can give a sharp peak in the spectrum. Another trace appears around 3 MHz when the angle is 20−70°. This trace is less intense, but also shows a gradual variation in frequency. This trace must correspond to the weak but sharp peak observed at 2.7 MHz in the spectrum. The remaining trace is the most intense, but its frequency is rather strongly dependent on the angle. Thus this gives the broad peak centered ∼2.5 MHz seen only in the simulation. Since this peak is too broad, the corresponding echo modulation must decay within the dead time. For this complex, unfortunately, all the peaks resolved in the spectrum come from the off-axis components. Thus it seems impossible to estimate parameters only from an inspection of the experimental spectrum.

The magnitude of HFC of 5−8 MHz found for the VO^{2+}−^{14}N system is much smaller than that for Cu^{2+}−^{14}N system.[43] In square-planar Cu^{2+} complexes, the unpaired electron occupies the $d_{x^2-y^2}$ orbital (when the ligand atoms are on the *x* and *y* axes). Because this orbital has sufficient overlap with the nitrogen lone-pair orbital, direct spin transfer from the d orbital to the nitrogen orbital would easily occur.[43] In VO^{2+} complexes, on the other hand, the unpaired electron occupies the d_{xy} orbital, and thus such direct spin transfer is unlikely.[44] The HFC of the VO^{2+}−N system is, however, much larger than that expected only from the dipole−dipole coupling mechanism.[19] Such a size of HFC would be well understood in terms of indirect spin transfer mechanism, where the nitrogen orbital is polarized by exchange interaction with the unpaired electron on the vanadium d orbital.[45] Since the β spin electron on the nitrogen lone-pair orbital receives more Coulomb repulsion from the unpaired α spin electron on the vanadium, a negative spin is expected to be induced on the lone-pair orbital. Thus the **A** tensor components must be negative. Since the lone-pair orbital $|n\rangle$ is an sp^n hybrid, this orbital can be expressed as

$$|n\rangle = c_s|N2s\rangle + c_{pZ}|N2p_Z\rangle$$

where $c_s^2 + c_{pZ}^2 = 1$. Then the **A** tensor components can be divided into three parts as (with neglect of the rhombicity of HFC)

$$A_X = A_Y = A_{iso} - A_{pZ} - A_{dd}$$

$$A_Z = A_{iso} + 2A_{pZ} + 2A_{dd}$$

where

$$A_{iso} = \rho_n c_s^2 A_0(N2s) \quad (10)$$

$$A_{pZ} = \rho_n c_p^2 A_0(N2p) \quad (11)$$

Here ρ_n is the spin population of the nitrogen lone-pair orbital. The symbols A_0(N2s) and A_0(N2p) denote the HFC parameters expected when the unit spin is on the nitrogen 2s and 2p orbitals, respectively, and A_0(N2s) = 1811 and A_0(N2p) = 55.5 MHz.[46] The symbol A_{dd} denotes the dipolar coupling between the unpaired electron on vanadium and the nitrogen nuclear spin

Table 2. Decomposition of Vanadium−^{14}Nitrogen Hyperfine Coupling into Contributions from Indirect Spin Transfer (A_{iso} and A_{pZ}) and Dipole−Dipole Coupling (A_{dd})

	A_{iso}/ MHz	c_s^2	ρ_n/ %	A_{pZ}/ MHz	A_{dd}/ MHz	*r*/Å	X-ray data *r*/Å	ref
VO(edda)	−4.98	1/4	−1.10	−0.46	0.58	2.15		
$VO(gly)_2$	−5.10	1/4	−1.13	−0.47	0.67	2.04	2.132	*c*
VO(salen)	−5.83	1/3	−0.97	−0.36	0.62	2.09	2.053	*d*
VO(salophen)	−5.78	1/3	−0.96	−0.35	0.65	2.07		
$VO(NCS)_4^{2-}$	−7.47	1/2	−0.82	−0.23	0.66	2.05	2.04	*e*
$VO(meox)_2$[a]	−6.27	1/3	−1.04	−0.38	0.66	2.05	2.136	*f*
$VO(min)Cl^+$ [a]	−6.43	1/3	−1.07	−0.39	0.61	2.11	2.122	*g*
VO(oep)[b]	−7.2	1/3	−1.19	−0.44	0.69	2.02	2.102	*h*

[a] Reference 19. [b] Reference 21. [c] Reference 48. The V−N_{amine} distance in $(Me_4N)[VO(L\text{-histidine})(NCS)_2]\cdot H_2O$. [d] Reference 49. [e] Reference 30. [f] Reference 50. [g] Reference 51. [h] Reference 52.

and can be expressed as

$$A_{dd} = \frac{\mu_0}{4\pi}\frac{g_e\mu_B g(^{14}N)\mu_N}{hr^3}$$

$$= 5.70 \times (r/Å)^{-3}\ (MHz) \quad (12)$$

where *r* is the V−N bond distance. Since the unpaired electron must be predominantly on the vanadium d_{xy} orbital, we have set the spin population of the d_{xy} orbital at the unity in eq 12. The spin population of the nitrogen lone-pair orbital can be readily estimated from eq 10, where we set $c_s^2 = 1/4$ for sp^3-hybrid amine nitrogen, $c_s^2 = 1/3$ for sp^2-hybrid imine nitrogen,[47] and $c_s^2 = 1/2$ for sp-hybrid NCS^- nitrogen. The estimated spin populations are listed in Table 2, where the signs of the principal **A** values are set minus based on the prediction of the indirect spin transfer mechanism. The resulting values are all around −1% with a slight difference of amine > imine > NCS^- in magnitude. It may be noted that this order is in accordance with the order of the basicities of the ligands. The lone-pair orbital also has p-orbital character, and this contributes to the anisotropic part of the **A** tensor. With use of the above estimated ρ_n values, one can estimate $A_{pZ} = -0.47$ to -0.23 MHz from eq 11 (Table 2). The remaining anisotropy can be attributed to the dipole−dipole coupling. Before estimating the remaining anisotropy, however, we must mention the axis assignments made in the simulation because the *Y* and *Z* axes are experimentally indistinguishable. Equation 12 shows that the magnitude of A_{dd} is always larger than the magnitude of the above estimated A_{pZ}: $A_{dd} = 0.54-0.7$ MHz when *r* is in the likely range of 2.2−2.0 Å. Thus A_Z, the component along the V−N bond, is expected to be the largest of the three principal components. Since the *A* values must be negative, the principal value having the smallest magnitude must correspond to the *Z* component. This is the criterion which we followed in the simulation. By subtracting A_{iso} and $2A_{pZ}$ from A_Z, we can estimate the contributions of the dipole-dipole coupling, and further the V−N bond distances using eq 12 (Table 2). We

(43) Brown, T. G.; Hoffman, B. M. *Mol. Phys.* **1980**, *39*, 1073−1109.
(44) Mulks, C. F.; van Willigen, H. *J. Phys. Chem.* **1981**, *85*, 1220−1224.
(45) Scholes, C. P.; Falkowski, K. M.; Chen. S.; Bank, J. *J. Am. Chem. Soc.* **1986**, *108*, 1660−1671.
(46) Atherton, N. W. *Principles of Electron Spin Resonance*; Ellis Horwood and Prentice Hall: London, 1993.

(47) One may expect $c_s^2 = \cot^2\theta = 0.528$ (θ is the half of the C=N−C angle)[37] for five-membered ring nitrogens such as imidazole and pyrrole, where $2\theta = 108°$. However, this c_s value has given unreasonable V−N bond distances. This presumably indicates that the hybridization ratio does not varies so drastically with the C=N−C angle. Unfortunately we could not decide an appropriate value, so that we tentatively used $c_s^2 = 1/3$ for the imidazole and pyrrole nitrogen as well as for the six-membered ring nitrogens. The tentative value, interestingly, has given a reasonable estimate for the V−N bond distance of $VO(min)_4Cl^+$ (Table 2). On the contrary, the agreement is not very good for VO(oep). For this complex, $c_s^2 = 0.38$ can be obtained when calculated reversely from the experimental V−N bond distance.

also performed the same analysis for some literature data,[19,21] and the results are included in Table 2. The resulting r values are in agreement with the X-ray determined V−N bond distances,[30,48−52] validating the indirect spin transfer mechanism. This analysis provides valuable insights into the origin of the good correlation between the HFC parameters and nitrogen types. The analysis shows that the polarizations of the lone-pair orbitals are invariably around −1%. On the other hand, the sp^n hybridization ratio should vary largely from $^1/_4$ to $^1/_2$, depending on the type of nitrogen. This explains the good correlation between the HFC parameters and nitrogen types.

The **A** tensors additionally show the rhombicity of $A_X \neq A_Y$. There would be two possible mechanisms responsible for the rhombicity: One mechanism is based on indirect spin transfer to the nitrogen π orbital. Such indirect spin transfer will induce a negative spin on the nitrogen π orbital and add $2A_\pi$ and $-A_\pi$ ($A_\pi < 0$) to the **A** tensor components parallel and perpendicular to the π orbital, respectively. For VO(salen) and VO(salophen), where the π orbital is along the A_X axis, this mechanism predicts $A_X < A_Y$. This is consistent with the ESEEM results. The other mechanism is based on the direct spin transfer. This may occur because of the nonzero overlap of the vanadium d_{xy} orbital with the nitrogen in-plane p orbital (p_y orbital when the nitrogen atom is on the x axis). The unpaired electron delocalized slightly on the p_y orbital will give additional contributions of $2A_y$ and $-A_y$ ($A_y > 0$) to the **A** tensor components parallel and perpendicular to the p_y orbital, respectively. For VO(salen) and VO(salophen), where we have chosen the A_Y axis as parallel to the molecular frame y axis, this mechanism predicts the same relation $A_X < A_Y$. Although the two mechanisms are indistinguishable for VO(salen) and VO(salophen), they will become distinguishable when the C═N−C plane of the imine nitrogen is perpendicular to the equatorial plane. Such configuration occurs in VO(mim)$_4$Cl$^+$. (The X-ray data of an analogous complex, VO(1-vinyl-imidazole)$_4$Cl$^+$, are available.[44]) Reijerse *et al*.[19] reported that, for VO(mim)$_4$Cl$^+$, the **A** tensor axis for the smallest (largest in absolute value) component is perpendicular to the imidazole plane, i.e. in the molecular frame xy plane. They also reported that the corresponding axis in VO(meox)$_2$ is also perpendicular to the C═N−C plane, which is, on the contrary, parallel to the z axis[19] as in VO(salen) and VO(salophen). This exchange of the smallest component axis with respect to the molecular frame can only be explained in terms of the indirect spin transfer to the nitrogen π orbital. This may also explain the smaller rhomicity in the amine nitrogens.

According to the computer simulation, the A_Z and Q_Z axes (and also A_Y and Q_Y axes) are obviously misaligned in VO(edda) and VO(gly)$_2$ (Figure 10). Since the A_Z axis most likely coincides with the V−N bond direction, these findings suggest that the Q_Z axes of the edda^{2-} and gly$^-$ nitrogens are significantly deviated from their respective V−N directions. This suggestion, though seemingly unexpected, is in fact in line of the previous study by Ashby *et al*.[53] They proposed a model explaining the observed NQC tensors of metal-coordinated amine nitrogens. Their model shows that the NQC tensor axes of the amine nitrogens usually deviate from the M−N bond directions (except ammonia and possibly tertiary amines). This

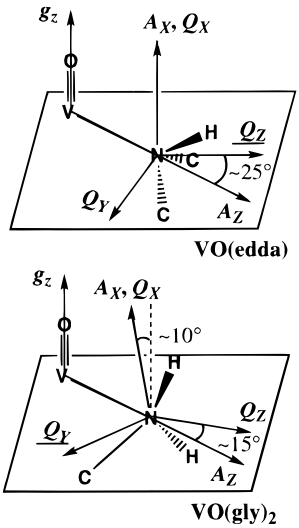

Figure 10. Possible orientations of the HFC **A** and NQC **Q** tensor axes of VO(edda) (top) and VO(gly)$_2$ (lower) based on the computer simulation of the ESEEM results. The unique axes of the NQC tensors are underlined.

is essentially because the local symmetry of amine nitrogen is only C_s even when the nitrogen has an idealized geometry. Thus the local symmetry only indicates that one NQC axis should be normal to the C_s mirror plane (M−N−C plane for primary amines and M−N−H plane for secondary amines) and the remaining two axes should be within this plane forming certain angles with the M−N bond. This is in contrast to the situation of imine nitrogen, where its idealized local symmetry is C_{2v} with the C_2 axis coincident with the M−N bond. Thus it is reasonable to expect that the NQC Q_Z axis coincides with the M−N bond direction and also with the HFC A_Z axis. In fact, in the simulation of VO(salen) and VO(salophen), no evidence was found for the misalignment of the HFC and NQC tensors.

In closing, we mention possible exceptions to the correlation rule. To the best of our knowledge, a VO−hydrotris(3,5-dimethyl-1-pyrazolyl)borate complex is the only VO^{2+} complex hitherto reported to exhibit an exceptional ^{14}N HFC parameter, $|A_{iso}| = 1.7$ MHz.[18] However, the pyrazole moiety contains two nitrogens, where one nitrogen is directly coordinated to the VO^{2+} ion and the other nitrogen is a second neighbor of the VO^{2+} ion and attached to the boron atom. Unfortunately, it was not determined as to which nitrogen exhibits the observed ESEEM signal. Quite interestingly, this $|A_{iso}|$ value is in good agreement with that of the second-neighbor nitrogen in VO−hydroxamate complexes ($|A_{iso}| = 1.8$ MHz).[54] Since the ESEEM signal is expected to be most intense under exact cancelation conditions,[34] there remains a possibility that the ESEEM signal from the directly coordinating nitrogen is obscured by the observed signal. Of course, however, this does not exclude the other possibility that the coordinating nitrogen gives such a small HFC parameter owing to the significant distortion of the complex.[18] The HFC parameters of axially coordinated nitrogens are also controversial. Although $|A_{||}| = 13.2$ MHz for an axial nitrogen of VO−D-xylose isomerase was suggested by a previous ENDOR study,[55] this value was questioned by the subsequent ESEEM study,[24] which reports rather a usual value of $|A_{||}| = 5.7$ MHz ($|A_{iso}| = 6$ MHz) and suggests that this nitrogen derives from an equatorially coordinated imidazole. On the other hand, it has been suggested

(48) Li, X.; Zhou, K. *J. Crystallogr. Spectrosc. Res.* **1986**, *16*, 681−685.
(49) Riley, P. E.; Pecoraro, V. L.; Carrano, C.; Bonadies, J. A.; Raymond, K. N. *Inorg. Chem.* **1986**, *25*, 154−160.
(50) Shiro, M.; Fernando, Q. *Anal. Chem.* **1971**, *43*, 1222−1230.
(51) Calviou, L. J.; Arber, J. M.; Collison, D.; Garner, C. D.; Clegg, W. *J. Chem. Soc., Chem. Commun*. **1992**, 654−656.
(52) Molinaro, F. S.; Ibers, J. A. *Inorg. Chem*. **1976**, *15*, 2278−2283.
(53) Ashby, C. I. H.; Paton, W. F.; Brown, T. L. *J. Am. Chem. Soc*. **1980**, *102*, 2990−2998.
(54) Kofman,K.; Dikanov, S. A.; Haran, A.; Libman, J.; Shanzer, A.; Goldfarb, D. *J. Am. Chem. Soc.* **1995**, *117*, 383−391.
(55) Bogumil, R.; Hüttermann, J.; Kappl, R.; Stabler, R.; Sudfeldt, C.; Witzel, H. *Eur. J. Biochem.* **1991**, *196*, 305−312.

that the axially coordinated nitrogens may have a too small HFC value to be observed by ESEEM[18] or ENDOR[56] spectroscopy. Anyway, it must be recalled that indirect spin transfer mechanism itself does not guarantee the good correlation, and rather the occurrence of the nearly constant polarization of the nitrogen orbitals is responsible for the correlation. The polarization of the nitrogen orbital may depend on the position of the coordinating nitrogen relative to the V═O bond. For axially coordinated nitrogens, it is also likely that the *trans* effect lengthens the V−N bond distance and eventually reduces the polarization of the nitrogen orbital. Furthermore, the coexistence of strongly electron donating or withdrawing ligands may also affect the polarization of the nitrogen. Therefore it may be unsurprising if the correlation does not hold for such complexes.

Concluding Remarks

The present study has extended the correlation rule to the *sp*-hybrid nitrogen and provided strong support for the idea that the types of nitrogens can be identified by means of ESEEM spectroscopy. We may provide the following criteria for the $VO^{2+}-{}^{14}N$ system: The $|A_{iso}|$ values are (1) ∼5 MHz for amine nitrogens, (2) ∼6−7 MHz for imine nitrogens, and (3) ∼7.5 MHz for the NCS^- nitrogen. The analysis based on the indirect spin transfer mechanism has shown that this good correlation is due to the fact the sp^n hybridization ratio of the nitrogen lone-pair orbital is inherent to the type of nitrogen. Of the three types of nitrogens, the *sp*-hybrid NCS^- nitrogen has the largest magnitude of HFC, followed by the sp^2-hybrid imine nitrogens and the sp^3-hybrid amine nitrogens in accordance with the order of the s-orbital contents in the sp^n-hybrid orbitals. It is also important to note that the good correlation is largely owed to the nearly constant polarization of the nitrogen lone-pair orbitals. This, in other words, suggests that, if the polarization is affected by significant geometry distortion or coexistence of strongly electron donating/withdrawing ligands, the correlation rule may be violated.

(56) Kirste, B.; van Willigen, H. *J. Phys. Chem.* **1982**, *86*, 2743−2749.

IC961462+